Trailing edge noise prediction for rotating blades: analysis and comparison of two classical approaches

S. Sinayoko*,
Department of Engineering, University of Cambridge
M. Kingan†,
Institute of Sound and Vibration, University of Southampton
A. Agarwal ‡
Department of Engineering, University of Cambridge

Different versions of Amiet's theory are used for predicting trailing edge noise radiation from rotating blades, for non-compact sources. It is not known which version is the correct one, and what the range of validity of the theory is. This paper derives Amiet's theory and compares it to a different approach based on the Ffowcs-Williams and Hawkings analogy. Both theories are applied to model blade elements of a wind turbine, a cooling fan and an aircraft propeller. The sound pressure levels obtained using the two approaches are within 1 dB of each other at high enough frequency (Helmholtz number relative to chord bigger than 1) and for chordwise Mach numbers lower than 0.9. The correct form of Amiet's theory is identified. It can be used over a broad range of frequencies and Mach numbers to predict trailing edge noise radiation from rotating blades.

Introduction

Trailing edge noise, is well understood for a fixed blade in a uniform flow. Although a model, by Amiet, exists for trailing edge noise from rotating blades, this model has not been validated independently. Moreover, different authors use different versions of the same model, and it is not known which version is the correct one. This paper identifies the correct version of Amiet's model and presents an alternative approach. The models presented in this paper are applicable to a wide range of problems, including wind turbines, cooling fans, aircraft propellers and helicopters.

Amiet[1–3] showed how to model trailing edge noise in the frequency domain for a static blade in uniform flow. His model describes how the hydrodynamic waves convecting within the boundary layer are scattered by the trailing edge, thereby generating unsteady loads over the surface of the blade. These unsteady loads generate noise efficiently (scales with M^5). Amiet's model, however, is restricted to high frequencies (relative to the chord, i.e. for $kc > 1$), because its solution of the scattering problem assumes that the blade is semi-infinite. Roger at al[4,5] extended Amiet's model to lower frequencies by taking into account the backscattering from the leading edge.

Amiet[6,7] proposed a simple model for predicting trailing edge noise from rotating blades. First, one estimates the instantaneous power spectral density radiating from the blade, while it is located at a particular azimuthal angle around the rotor. Second, the power spectra are averaged around the azimuth. In that process, each spectrum is weighted by a Doppler factor, of the form $(\omega', \omega)^a$, where ω' denotes the source frequency and ω the observer frequency. The exponent a takes the value 1 in,[3,8] 2 in[7] and -2 in.[9] This paper identifies the correct value of a.

An alternative approach for predicting trailing edge noise is to consider the noise radiating from a rotating dipole and to use a Green's function. This is the approach used by Kim and George.[10] However, their study

*Research Associate, Department of Engineering, University of Cambridge
†Lecturer, ISVR, University of Southampton
‡Lecturer, Department of Engineering, University of Cambridge

assumes that the blade is compact. We extend their work and present a model that is valid for a non-compact source.

This paper builds on the work of Blandeau and Joseph,[11] who compared Amiet's model and a non-compact version of Kim-George's model. They obtained a good agreement between both models and defined the range of validity of Amiet's model. However, the mean flow and spanwise wavenumber were neglected in their study. The range of validity of Amiet's approach they proposed may not hold when the mean flow is taken into account. Both mean flow and and spanwise wavenumber will be taken into account in this paper.

I. Trailing edge noise theory for isolated airfoils

A. Introduction

The most successful model for trailing edge noise was developed by Amiet.[2,3,12] The turbulent boundary layer is modelled in the frequency domain as a series of waves travelling towards the trailing edge. Each wave is scattered at the trailing edge, giving rise to an upstream travelling wave. This upstream travelling wave is such that the total pressure vanishes downstream of the flat plate (in the plane of the flat plate). The presence of the scattered wave creates an unsteady loading on the blade, which generates noise. A clear derivation of Amiet's model has been proposed by Roger and Moreau.[4] In the following, we present the main results of this theory, that is the far field power spectral density (PSD) for trailing edge noise radiating from a flat plate in a uniform flow at zero angle of attack.

B. Power spectral density for trailing edge noise

Consider a flat plate in a uniform flow of Mach number M at zero angle of attack. The observer location is expressed using a cartesian coordinate system (x, y, z), with x in the chordwise direction and pointing downstream and z in the vertical direction. The PSD at frequency ω is given by[3,12]

$$S_{pp}(\omega) = \left(\frac{\omega}{c_0}\frac{c}{2}\frac{z}{2\pi\sigma^2}\right)^2 \frac{s}{2}|\Psi_L(k_X, k_y, k_c)|^2 l_y(k_X, k_y) S_{qq}(\omega), \tag{1}$$

where c is the blade chord length, s the span of the plate, c_0 the speed of sound,

$$\sigma^2 = x^2 + \beta^2(y^2 + z^2), \qquad \beta^2 = 1 - M^2, \qquad U_c = 0.8 M c_0, \tag{2}$$

$$\tag{3}$$

and l_y is the spanwise correlation length, defined as[4]

$$l_y(k_X, k_y) \equiv \frac{1}{k_X}\frac{\eta}{\eta^2 + (k_y/k_X)^2}. \tag{4}$$

In (4), η is the exponential decay rate of the spanwise coherence function[13] ($e^{-\eta(k_y/k_X)}$). A typical value for η is 1/2.1.

The term $k_X = \omega/U_c$ denotes the wavenumber associated with the hydrodynamic gusts convecting towards the trailing edge at speed U_c (assuming frozen turbulence). The terms k_y and k_c denote the spanwise wavenumber and the coupling wavenumber (between the hydrodynamic near field and the acoustic far field). For a stationary flat plate in a uniform flow, these three wavenumbers are given by[1]

$$k_X = \frac{\omega}{U_c}, \qquad k_y = \frac{\omega}{c_0}\frac{y}{\sigma}, \qquad k_c = \frac{\omega}{c_0\beta^2}\left(M - \frac{x}{\sigma}\right). \tag{5}$$

The functions Ψ_L and S_{qq} in (1) are the acoustically weighted blade lift and the surface power spectral density respectively. Those two functions are discussed below.

C. Acoustic lift

General expression

The acoustic lift is given by

$$\Psi_L(X, k_X, k_y, k_c) = \frac{i}{A}\left\{\sqrt{\frac{B}{B-A}}\mathrm{erf}\Big((1+i)\sqrt{B-A}\Big) + e^{i2A}\left[1 - \mathrm{erf}\Big((1+i)\sqrt{B}\Big)\right]\right\}, \tag{6}$$

where $k_X = \omega/U_c$,

$$A = k_X + k_c, \qquad B = k_X + \kappa + M\mu, \qquad \mu = Mk_X/\beta^2. \tag{7}$$

The wavenumber κ is a function of the spanwise wavenumber k_y. It is defined as

$$\kappa \equiv \begin{cases} \mu\sqrt{1-[k_y/(\beta\mu)]^2} & \text{if} \quad kr^2 < (\beta\mu)^2 \\ -i|\mu|\sqrt{[k_y/(\beta\mu)]^2-1} & \text{if} \quad kr^2 \geq (\beta\mu)^2 \end{cases} \tag{8}$$

so that the imaginary part of κ is always negative. This is required for the error functions in (6) to converge in the far field. The square roots in (6) has a branch cut along the negative imaginary axis, i.e. if $z = re^{i\theta}$ with $-\pi/2 < \theta \leq 3\pi/2$,

$$\sqrt{z} \equiv \begin{cases} \sqrt{r}e^{i\theta/2} & \text{if} \quad -\pi/2 < \theta \leq \pi/2, \\ -\sqrt{r}e^{i\theta/2} & \text{if} \quad \pi/2 < \theta \leq 3\pi/2. \end{cases} \tag{9}$$

Using the above definitions, the acoustic lift is such that

$$\Psi_L(X, -k_X, -k_y, -k_c) = \Psi_L^\star(X, k_X, k_y, k_c), \tag{10}$$

where $\Psi_L^\star$ is the complex conjugate of Ψ_L.

D. Surface pressure power spectral density

The PSD of the incoming pressure fluctuations at the trailing edge, denoted $S_{qq}(\omega)$, can be measured experimentally. If no experimental data is available, it can be estimated by using empirical low-order models. These low order models are expressed in terms of parameters characterizing the boundary layer, such as the boundary layer thickness, displacement thickness, wall shear stress etc. A review of the different models that are available can be found in Ref.[9]

In the rest of this report, we will use Kim-George's model, which gives

$$S_{qq}(\omega) = \frac{1}{2}\rho U_X^2 \frac{\delta^*}{U_X} F(\tilde{\omega}), \tag{11}$$

where U_X is the chordwise Mach number and $\tilde{\omega} = \omega\delta^*/U_X$,

$$\delta^* = \begin{cases} c(24.3 + 0.6625\chi) \times 10^{-4}, & \text{if} \quad \chi \leq 4^\circ \\ c(26.95 + 0.6625(\chi-4) + 0.3044(\chi-4)^2 + 0.0104(\chi-4)^3) \times 10^{-4}, & \chi > 4^\circ. \end{cases} \tag{12}$$

where χ denotes the angle of attack, and

$$F(\tilde{\omega}) = \begin{cases} \dfrac{1.732 \times 10^{-3}\tilde{\omega}}{1 - 5.489\tilde{\omega} + 36.74\tilde{\omega}^2 + 0.1505\tilde{\omega}^5} & \text{if} \quad \tilde{\omega} < 0.06, \\ \dfrac{1.4216 \times 10^{-3}\tilde{\omega}}{0.3261 + 4.1837\tilde{\omega} + 22.818\tilde{\omega}^2 + 0.0013\tilde{\omega}^3 + 0.0028\tilde{\omega}^5} & \text{if} \quad \tilde{\omega} \geq 0.06. \end{cases} \tag{13}$$

II. Results

A. Acoustic lift

The magnitude (or squared magnitude) of the acoustic lift is plotted in figures 1 and 2, as a function of frequency and spanwise wavenumber k_y respectively, for $M = 0.1$. In both figures, the acoustic wavenumber k_c is defined assuming that $x/\sigma = 0.7$.

Figure 1 shows that $|\Psi|^2$ varies as $1/\omega^2$, and that it drops by up to 10 dB when going from $k_y = 0$ (circles) to $k_y = \infty$ (squares). The magnitude of the drop is roughly independent of frequency.

Figure 2, shows how $|\Psi|$ varies with spanwise wavenumber, for a constant frequency of 1 kHz (solid line). The normalized spanwise wavenumber $k_y/\beta\mu$ is made to vary between 10^{-2} and 10^2. The transition between supercritical and subcritical gusts is at $k_y/\beta\mu = 1$. Typically, sharp increase occurs near $k_y/\beta\mu = 1$. That

transition is non-physical and occurs because the governing equation morphs from a Helmholtz equation to a Laplace equation. This was pointed out by Roger and Moreau,[4] who used a regularization technique to overcome this. Since Ψ is asymptotically constant at low and high values of k_y we define Ψ as a piecewise function, such that it is constant for supercritical gusts ($k_y/\beta\mu < 1$), and for highly subcritical gusts ($k_y/\beta\mu > 10$). Between those values, we use a linear interpolation in terms of $\log_{10} k_y/\beta\mu$. The piecewise implementation of $|\Psi|^2$ is shown as a dashed line in the figure 2.

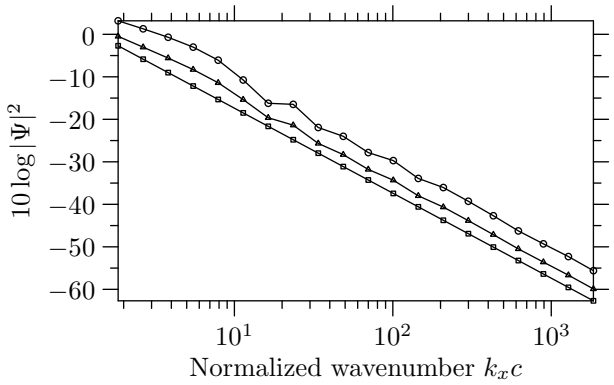

Figure 1: Acoustic lift $|\Psi(k_x, k_y, k_c)|^2$ in decibels as a function of frequency, at Mach $M = 0.1$. The radiating wavenumber k_c is defined assuming an observer at $x/\sigma = 0.7$. Results are shown for $k_y = 0$ (circles), $k_y = 5\beta\mu$ (triangles) and $k_y = +\infty$ (squares). The acoustic lift energy decreases with frequency as $1/\omega^2$. It decreases by up to 10 dB going from supercritical to subcritical gusts.

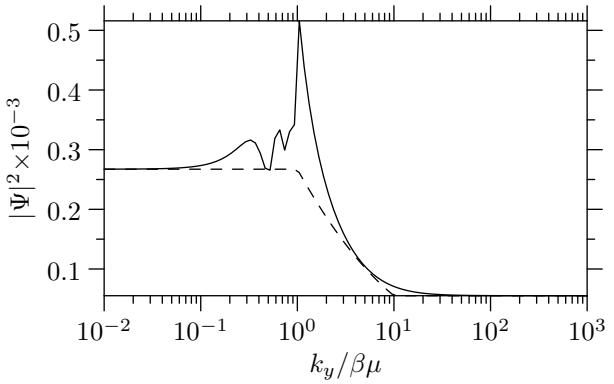

Figure 2: Acoustic lift energy $|\Psi(k_x, k_y, k_c)|^2$ in decibels as a function of k_y, at Mach $M = 0.1$ and frequency $f = 1000\,\text{Hz}$. The radiating wavenumber k_c is defined assuming an observer at $x/\sigma = 0.7$. The transition between supercritical and subcritical gusts is at $\overline{k}_y \equiv k_y/(\beta\mu) = 1$. The acoustic lift based on equation (6) becomes unphysical near the supercritical-subcritical transition[4] (solid line). We assume that Ψ is constant for $\overline{k}_y < 1$ and $\overline{k}_y$, and use a linear interpolation as a function of $\log_{10}(\overline{k}_y)$ for $1 \le \overline{k}_y \le 10$ (dashed line).

B. Directivity

The noise directivity, which we define as

$$D(\omega, \theta) = \frac{R^2}{s l_y(\omega)} \frac{S_{pp}(\omega, \theta)}{S_{qq}(\omega)}, \tag{14}$$

where $R = |\mathbf{x}|$, is plotted in figures 3 and 4. In both cases, the trailing edge is at $\theta = 0°$ and the leading edge at $\theta = 180°$.

Figure 3 shows the evolution of the directivity with frequency, for low and high Mach number. In both cases, the number of side lobes increases with frequency. Furthermore, at low frequencies ($kc = 1$, figure

3(a,d)), the directivity pattern is that of a dipole, with two main lobes towards $\pm 90°$. At low Mach number (figure 3(a-c)), the peak radiation angle moves towards the leading edge as frequency increases. At high Mach number (figure 3(d-f)), the peak radiation angle moves towards the trailing edge as frequency increases.

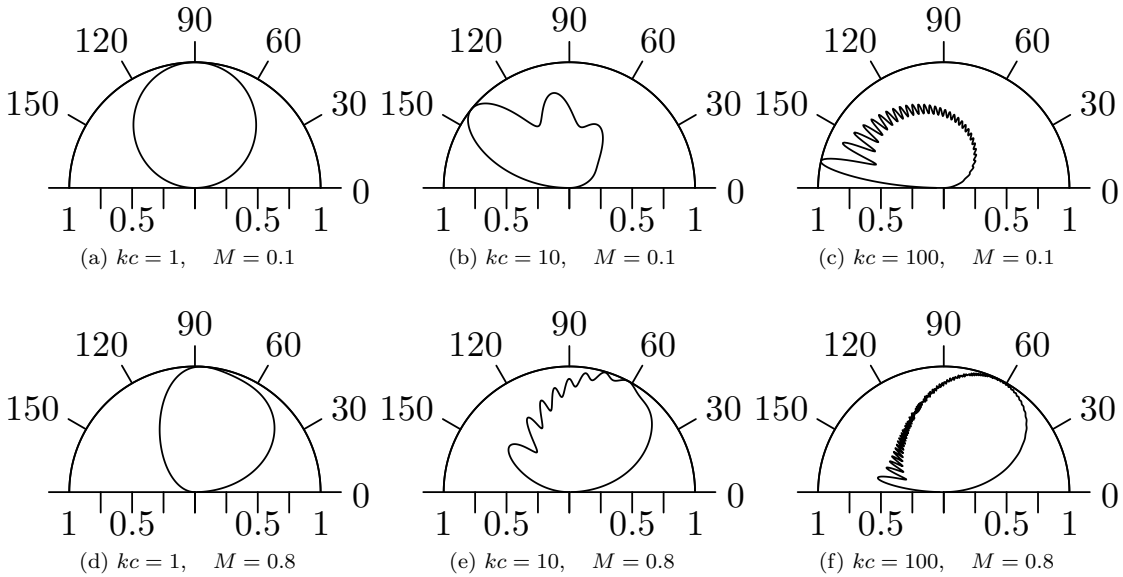

(a) $kc = 1, \quad M = 0.1$ (b) $kc = 10, \quad M = 0.1$ (c) $kc = 100, \quad M = 0.1$

(d) $kc = 1, \quad M = 0.8$ (e) $kc = 10, \quad M = 0.8$ (f) $kc = 100, \quad M = 0.8$

Figure 3: Trailing edge noise directivity as a function of frequency. The trailing edge is at 0° and the leading edge at 180°. Results are given in mid-plane ($y = 0$ and $k_y = 0$), at low Mach number ($M = 0.1$, top) and high Mach number ($M = 0.8$, bottom), for $k_y = 0$ and $kc = 1, 10, 100$ (low frequency to high frequency from left to right). At low Mach number, trailing edge noise is maximum in the forward arc and at high Mach number, in the rear arc. The number of side lobes increases with frequency.

Figure 4 shows the evolution of the directivity with the spanwise wavenumber k_y. At low Mach number (figure 4(a-c), the peak radiation angle moves towards the trailing edge and the radiation pattern becomes more dipole-like. At high Mach number (figure 4(d-f)) the peak radiation angle remains unchanged.

C. Validation

We validate our implementation for the far field PSD radiating from a stationary flat plate by comparing with published experimental data by Brooks and Hogdson.[13] The main input parameters are given below: In table 1, the observer location is in spherical coordinates. The origin is at the trailing edge of the plate,

observer (R, θ, ψ)	chord	span	U_c/U_X
$(1.22, \pi/2, \pi/2)$	0.61	span	0.6

Table 1: Brooks and Hodgson trailing edge noise experiment.

θ is the elevation angle from the x-axis (along the chord, pointing downstream), and ψ the azimuthal angle from the z-axis (orthogonal to the plate, pointing upwards).

Figure 5 shows the sound pressure level of trailing edge noise for the parameters of table 1, at Mach 0.11 and 0.2. The experimental measurements of Brooks and Hodgson[13] were used for both S_{qq} and l_y. The convection velocity was set to $U_c = 0.6U_X$. Agreement is good (less than 3 dB) at high frequency and poorer at low frequency (up to 5 dB).

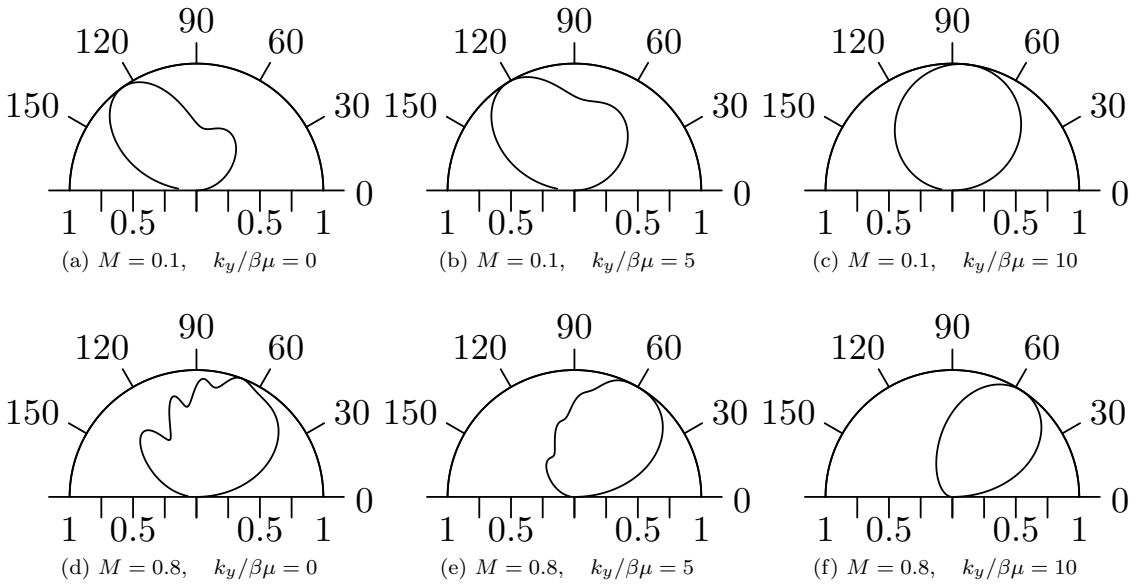

(a) $M = 0.1$, $k_y/\beta\mu = 0$ (b) $M = 0.1$, $k_y/\beta\mu = 5$ (c) $M = 0.1$, $k_y/\beta\mu = 10$

(d) $M = 0.8$, $k_y/\beta\mu = 0$ (e) $M = 0.8$, $k_y/\beta\mu = 5$ (f) $M = 0.8$, $k_y/\beta\mu = 10$

Figure 4: Trailing edge noise directivity as a function of k_y, moving from supercritical gusts ($k_y < \beta\mu$) to subcritical gusts ($k_y > \beta\mu$). The trailing edge is at 0° and the leading edge at 180°. Results are given at frequency $kc = 5$, at a low Mach number ($M = 0.1$, top) and a high Mach number ($M = 0.8$, bottom), for $k_y = 0, 5$ and 10. At low Mach number, the peak radiation angle moves towards 90° as k_y increases. At high Mach number, the side lobes are smoothed out as k_y increases and the peak radiation angles doesn't change.

III. Amiet's approach for rotating blades

A. Introduction

Coordinate systems

The observer coordinate system is defined as follows: the origin is at the hub, the z-axis is normal to the rotor plane and pointing against the wind; the (x, y) plane is the rotor plane and the x-axis points upwards. A flat plate is rotating in the rotor plane at rotational speed $\Omega = \dot{\gamma}t$, where γ is the angle between the x-axis and the leading edge. We use the polar coordinate system (r, γ) to describe the position of the blade in the (x, y) plane.

The vectors $\mathbf{e_x}$, $\mathbf{e_y}$, $\mathbf{e_z}$ are the unit vectors along the $x-$, $y-$, and $z-$axis respectively. Similarly, $\mathbf{e_r}$ and $\mathbf{e}_\gamma$ in the radial and tangential directions.

Objective

Given:

- the chord l,
- the pitch angle α, i.e. the angle between the rotor plane and the flat plate (see figure 6(a)),
- the angle of attack χ, i.e. the angle between the chord and the flow,
- the blade Mach number
$$\mathbf{M_t} = M_t \mathbf{e}_\gamma, \tag{15}$$
- the incident flow Mach number (see figure 6),
$$\mathbf{M} = -M_z \mathbf{e_z} + \mathbf{M_f}, \quad \text{where} \quad \mathbf{M_f} = -M_f(\cos\psi \mathbf{e_y} + \sin\psi \mathbf{e_x}) \tag{16}$$

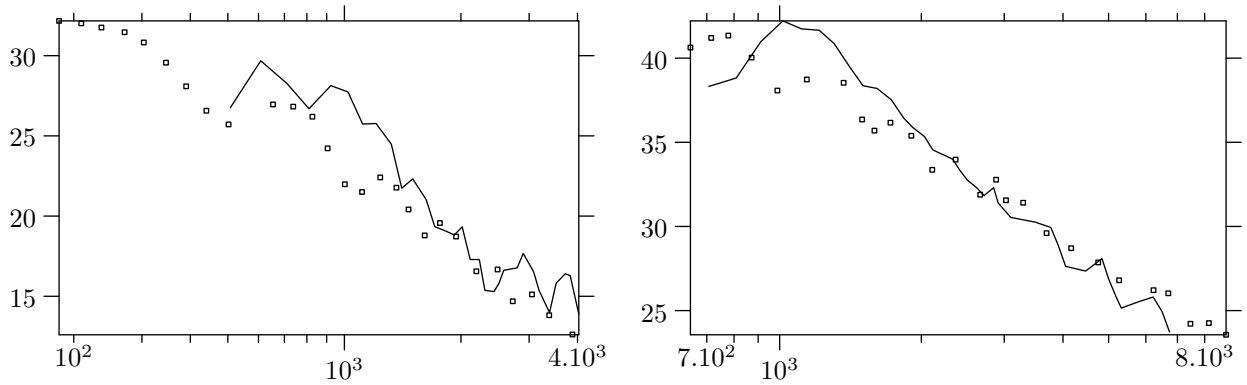

(a) $M = 0.11$ (b) $M = 0.2$

Figure 5: Numerical prediction and measurements of the sound pressure level at Mach 0.11 and 0.2 from Brooks and Hodgson.[13]

the aim is to express the pressure power spectral density (PSD) in the far field for trailing edge noise as a function of frequency ω and observer position $\mathbf{x_o} = (x_0, y_0, z_0)$.

Methodology

We follow the approach described by Schlinker and Amiet.[14] The idea is to express the PSD for a rotating flat plate in terms of the PSD for a flat plate in a wind tunnel. This is done by assuming that, during the time taken for the sound to travel from the source to the observer, the trailing edge is translating in a rectilinear manner. This approximation simplifies the derivation compared to the exact, Ffowcs-Williams and Hawkings approach.[9,15] It appears to be a very good approximation to predict the noise radiating from wind turbines.[9,11] The PSD for a flat plate in a wind tunnel is expressed analytically in terms of the chordwise Mach number by using the Schwartzschild method[2,3,12] or the Wiener-Hopf technique.[16]

B. Preliminary results

Chordwise Mach number

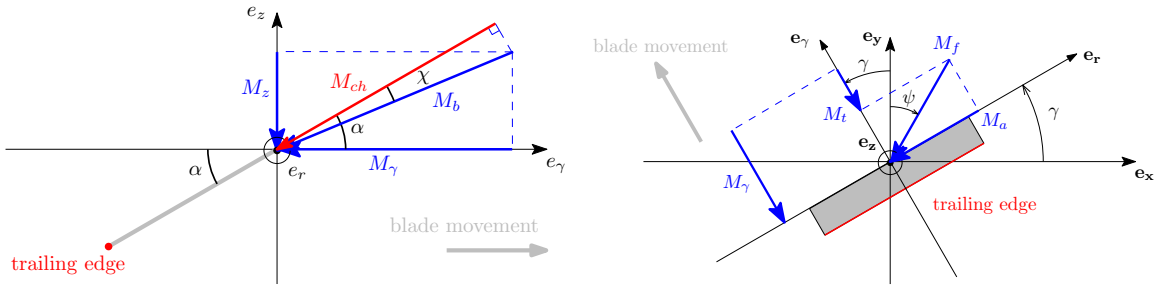

(a) Flat plate (in grey) in the $(\mathbf{e_\gamma}, \mathbf{e_z})$ plane, where $\mathbf{e_z}$ is pointing against the wind and is orthogonal to the rotor plane, and where $\mathbf{e_\gamma}$ is in the direction of rotation. The pitch angle (angle between rotor plane and flat plate) is α and the angle of attack is χ. The flow Mach number incident on the flat plate is $\mathbf{M_b} = -M_z\mathbf{e_z} - M_\gamma\mathbf{e_\gamma}$. The chordwise Mach number is $\mathbf{M_{ch}}$.

(b) Relationship between the flow Mach number M_γ along $\mathbf{e_\gamma}$, the blade Mach number M_t and the (wind) cross-flow M_f in the rotor plane $(\mathbf{e_x}, \mathbf{e_y})$. Note that the flat plate is not in the rotor plane (see Fig. 6(a)). The plate is shown in grey and the trailing edge in red. The angle $\gamma = \Omega t$ is the azimuthal angle, where Ω is the rotational speed of the rotor. The angle ψ gives the direction of the cross flow relative to $\mathbf{e_y}$.

Figure 6: Coordinate systems and Mach numbers around a flat plate moving in a uniform flow.

From figure 6(a), the chordwise Mach number $\mathbf{M_{ch}}$ is given by

$$\mathbf{M_{ch}} = -(M_\gamma - M_b \sin\alpha \sin\chi)\mathbf{e}_\gamma - (M_z + M_b \sin\chi \cos\alpha)\mathbf{e_z}, \tag{17}$$

$$M_b = \sqrt{M_\gamma^2 + M_z^2} \tag{18}$$

From figure 6(b),

$$M_\gamma = M_t + M_f \cos(\gamma + \psi), \qquad \mathbf{e}_\gamma = -\sin\gamma \mathbf{e_x} + \cos\gamma \mathbf{e_y}, \tag{19}$$

Coordinate system transformation from rotating blade to wind tunnel blade

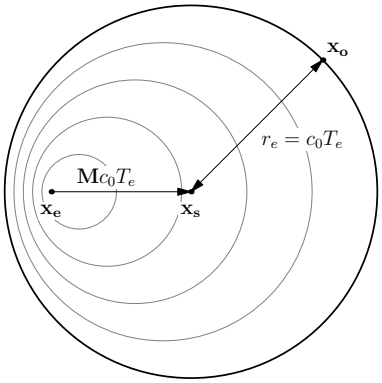

Figure 7: Original source position $\mathbf{x_e}$, retarded source position $\mathbf{x_s}$ and observer position $\mathbf{x_o}$ in emission coordinates (i.e. relative to the retarded source position at reception time) in a uniform flow of Mach $\mathbf{M}$. The retarded source position is independent of the observer velocity[17] at reception time, and depends only on its position. The circles indicate snapshots of the wavefront emitted from $\mathbf{x_e}$ at $t = 0$ and reaching $\mathbf{x_o}$ at $t = T_e$.

Present source position and retarded source position For a rotating blade, the retarded source position is defined as follows. After emitting sound (at $t = 0$) at the trailing edge $\mathbf{x_e}$, the source eddy is convected with the flow (at Mach $\mathbf{M}$). The retarded source position $\mathbf{x_s}$ is the position of the eddy at reception time ($t = T_e$), i.e. when the wave front reaches the observer position $\mathbf{x_o}$. From figure 7, the retarded source position is given by

$$\mathbf{x_s} = \mathbf{x_e} + \mathbf{M}c_0 T_e. \tag{20}$$

If T_e is small compared to the rotation period of the turbine, we can approximate the rotation of the blade during T_e as a rectilinear translation. We model the rotation of a blade element, centred around the emission position $\mathbf{x_e}$, as a translation at the chordwise Mach number $-\mathbf{M_{ch}}$. In a coordinate system attached to the blade element, the flow Mach number is uniform and equal to $\mathbf{M_{ch}}$, which corresponds to the wind tunnel case.

We now derive the corresponding reception coordinate formulae for the wind tunnel case. For a sound wave emitted at the origin (located at the trailing edge) at $t = 0$ and travelling in a uniform flow of Mach $\mathbf{M_{ch}}$, the retarded source position $\mathbf{x_s'}$ is given by

$$\mathbf{x_s}' = \mathbf{M_{ch}} c_0 T_e. \tag{21}$$

In the wind tunnel case, if $\mathbf{x}$ denotes the observer location with respect to the trailing edge (reception coordinates), and $\mathbf{x}'$ the observer location with respect to the retarded source position (retarded coordinates), we have (see figure 7 with $\mathbf{x_e} = 0$, $\mathbf{x_s} = \mathbf{x_s'}$ and $\mathbf{x_o} = \mathbf{x}$).

$$\mathbf{x} = \mathbf{x}' + \mathbf{x_s}' = \mathbf{x}' + \mathbf{M_{ch}} c_0 T_e. \tag{22}$$

The expressions derived for the wind tunnel case can now be applied to a rotating blade element by substituting $\mathbf{x}'$ by $\mathbf{x}_o - \mathbf{x}_s$ in equation (23), i.e. from (20),

$$\mathbf{x} = \mathbf{x}_o - [\mathbf{x_e} + (\mathbf{M} - \mathbf{M_{ch}}) c_0 T_e]. \tag{23}$$

This is allowed because the instantaneous pressure is independent of the movement of the observer relative to the source.[17] In the above equation $\mathbf{x}$ is the observer position in reception coordinates, i.e. with respect to the present source location. The present source location $\mathbf{x}_p$ for a rotating blade is therefore given by

$$\mathbf{x_p} = \mathbf{x_e} + (\mathbf{M} - \mathbf{M_{ch}})c_0 T_e. \tag{24}$$

The source position at emission time satisfies $|\mathbf{x_e}| \leq L$, where L is the blade span, while $T_e \to +\infty$ in the far-field, therefore (provided that $\mathbf{M} \neq \mathbf{M_{ch}}$ i.e. $\mathbf{M_t} \neq 0$)

$$\mathbf{x_p} \approx (\mathbf{M} - \mathbf{M_{ch}})c_0 T_e, \quad \text{(observer in the far field)}. \tag{25}$$

For an observer in the far field, we can assume $\mathbf{x_e} = 0$, i.e. that the source is located at the hub. The above result is analogous to the one derived by Schlinker and Amiet[14] (equation (46)).

The present source position $\mathbf{x}_p$ is a function of the retarded time T_e, which can be computed by observing that

$$(c_0 T_e)^2 = |\mathbf{x_o} - \mathbf{x_s}|^2 \approx |\mathbf{x_o} - \mathbf{M}c_0 T_e|^2. \tag{26}$$

The above equation leads to a second order polynomial equation for T_e which can be solved numerically.

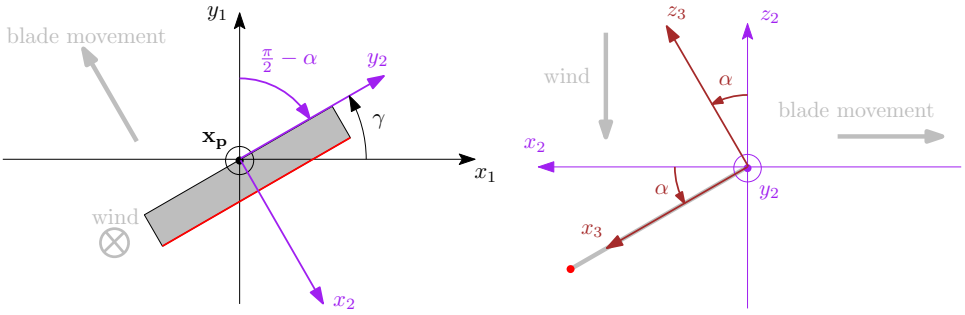

(a) (x_2, y_2, z_2) is obtained by rotating the (x_1, y_1, z_1) by $\pi/2 - \gamma$ around the z_1-axis.

(b) (x_3, y_3, z_3) is obtained by rotating (x_2, y_2, z_2) by α around the y_2-axis.

Figure 8: Coordinate systems (x_1, y_1, z_1), centred on the present source position $\mathbf{x_p}$, (x_2, y_2, z_2), such that y_2 is in the spanwise direction, and (z_3, y_3, z_3), such that y_3 is in the spanwise direction and x_3 in the chordwise direction.

CHANGE OF COORDINATE SYSTEM The observer position must be expressed in a coordinate system attached to the present source position $\mathbf{x_p}$, and such that

- the y-axis is pointing spanwise
- the x-axis is pointing chordwise

Let $\mathbf{x_1} = (x_1, y_1, z_1)$ denote the coordinate system centred on the present source position. We have

$$\mathbf{x_1} = \mathbf{x_0} - \mathbf{x_p} \tag{27}$$

We want the y-axis to point in the spanwise direction, i.e. in the radial direction $\mathbf{e_r}$. This can be done by rotating the $\mathbf{x_1}$-coordinate system by $\pi/2 - \alpha$ around the z_1-direction (figure 8(a)):

$$\begin{pmatrix} x_2 \\ y_2 \\ z_2 \end{pmatrix} = \begin{pmatrix} \sin\gamma & -\cos\gamma & 0 \\ \cos\gamma & \sin\gamma & 0 \\ 0 & 0 & 1 \end{pmatrix} \begin{pmatrix} x_1 \\ y_1 \\ z_1 \end{pmatrix} \tag{28}$$

Finally, the x-axis must point in the chordwise direction. Since the blade makes an angle α with the rotor plane (with normal e_z), we get the correct coordinate system $\mathbf{x_3} = (x_3, y_3, z_3)$ is given by rotating $\mathbf{x_2}$ by α around y_2 (figure 8(b)), i.e.

$$\begin{pmatrix} x_3 \\ y_3 \\ z_3 \end{pmatrix} = \begin{pmatrix} \cos\alpha & 0 & -\sin\alpha \\ 0 & 1 & 0 \\ \sin\alpha & 0 & \cos\alpha \end{pmatrix} \begin{pmatrix} x_2 \\ y_2 \\ z_2 \end{pmatrix} \tag{29}$$

Doppler shift

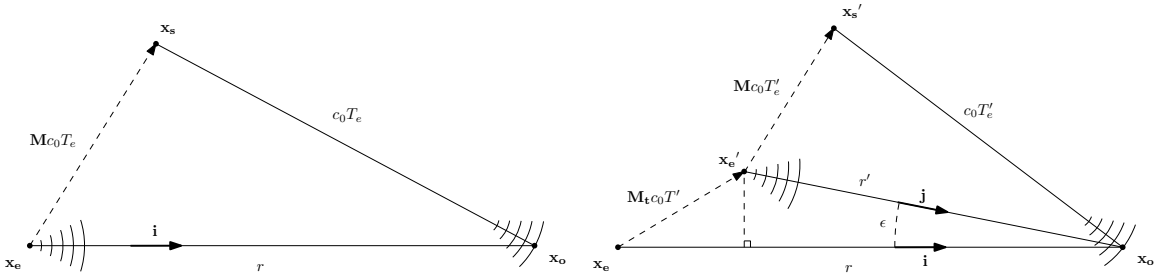

(a) Sound at frequency ω' emited from $\mathbf{x_e}$ at $t = 0$ and arriving at $\mathbf{x_0}$ at $t = T_e$.

(b) Sound at frequency $\omega' = 2\pi/T'$ emited from $\mathbf{x_e'}$ at $t = T'$ and arriving at $\mathbf{x_0}$ at $t = T' + T_e'$.

Figure 9: Two sound bursts are emitted at $t = 0$ (top figure) and $t = T'$ (bottom figure), from $\mathbf{x}_e$, where T' is the period sound source. To the observer $\mathbf{x}_o$, the sound appears to originate from the retarded position ($\mathbf{x}_s$ at $t = T_e$ and $\mathbf{x}_s'$ at $t = T' + T_e'$). Since the source is moving between the two bursts, the period perceived by the observer, i.e. the time interval between the reception times of the two sound bursts ($t = T_e$ and $t = T' + T_e'$), is different from T': this phenomenon is called Doppler shift.

As explained by Amiet,[17] the Doppler shift (see figure 9) is given by

$$\frac{\omega}{\omega'} = 1 + \frac{(\mathbf{M_t} \cdot \mathbf{i})}{1 + (\mathbf{M} - \mathbf{M_t}) \cdot \mathbf{i}}, \quad \text{(far field)}, \tag{30}$$

where $\mathbf{M}$ and $\mathbf{M}_t$ are respectively the flow Mach number and the source Mach number relative to the observer, and $\mathbf{i}$ is the unit vector from the emission position (the source position at emission time) to the observer position.

Physical interpretation relative to the speed of time The Doppler shift indicates how the frequency of a pure tone varies for a moving observer (relative to the source), compared to a fixed observer. Following Amiet,[17] an alternative physical interpretation can be obtained by observing that, for a pure tone, the pressure p' for a fixed observer and p for a moving observer are given by

$$\begin{cases} p'(t) = e^{-i\omega' t} \\ p(t) = e^{-i\omega t} \end{cases}, \quad \text{so} \quad p(t) = e^{-i\omega'(\omega/\omega')t} = p'\left((\omega/\omega')t\right), \tag{31}$$

where ω' is the source frequency and ω the frequency received by the moving observer. The above equation implies that the measurement of the pressure time history is sped up (or slowed down), by a factor ω/ω', for a moving observer, compared to a fixed observer.

Power spectral density in two reference frames

From equation (31), the autocorrelations $R'_{pp}(t)$ and $R_{pp}(t)$ for a fixed observer and a moving observer (relative to the source), are such that

$$R_{pp}(t) = \lim_{T\to+\infty} \frac{1}{2T} \int_{-T}^{T} p(\tau)p(t-\tau)\, d\tau = \lim_{T\to+\infty} \frac{1}{2T} \int_{-T}^{T} p'(a\tau)p'(a(t-\tau))\, d\tau \tag{32}$$

$$= \lim_{T\to+\infty} \frac{1}{2aT} \int_{-aT}^{aT} p'(\tau')p'(at-\tau')\, d\tau' = R'_{pp}(at), \tag{33}$$

where $a = \omega/\omega'$.

Since the power spectral density (PSD) is defined as the Fourier transform of the autocorrelation, the PSD $S_{pp}(\omega)$, for a moving observer, is related to the PSD $S'_{pp}(\omega')$ for a fixed observer by

$$S_{pp}(\omega) = \int_{-\infty}^{+\infty} R_{pp}(t)e^{i\omega t}\, dt = \int_{-\infty}^{+\infty} R'_{pp}(at)e^{i\omega' at}\, dt = \frac{1}{a} S'_{pp}(\omega'), \tag{34}$$

i.e.

$$S_{pp}(\omega) = \frac{\omega'}{\omega} S'_{pp}(\omega'). \tag{35}$$

C. Amiet's model

Azimuthal averaging

The PSD measured at the observer location at frequency ω, in the coordinate system attached to the hub, can be expressed by averaging the instantaneous PSD $S_{pp}(\omega, \gamma)$, radiating at frequency ω from the blade located at angle γ, over a complete rotation of the rotor blade, i.e.

$$S_{pp}(\omega) = \frac{1}{T_\Omega} \int_0^{T_\Omega} S_{pp}(\omega, \gamma)\, dt, \tag{36}$$

where $T_\Omega = 2\pi/\Omega$. Let n be the number of (sound) periods measured at the observer location in time dt: we have $dt = n2\pi/\omega$. The time taken for the source to generate those n cycles, is $dt' = n2\pi/\omega'$, where ω' is the frequency of the source, so $dt = (\omega'/\omega)dt'$. Furthermore, we can express dt' in terms of the azimuthal angle increment $d\gamma$ covered by the blade during the emission time: $dt' = \text{distance/velocity} = rd\gamma/r\Omega$, where r is the radial location along the blade. We hence have

$$dt = \frac{\omega'}{\omega} \frac{d\gamma}{\Omega}, \tag{37}$$

and

$$S_{pp}(\omega) = \frac{1}{2\pi} \int_0^{2\pi} \frac{\omega'}{\omega} S_{pp}(\omega, \gamma)\, d\gamma. \tag{38}$$

From equation (35), the PSD in the integrand of equation (38) can be expressed as

$$S_{pp}(\omega, \gamma) = \frac{\omega'}{\omega} S'_{pp}(\omega', \gamma), \tag{39}$$

where S'_{pp} is the PSD in the wind tunnel reference frame, which is attached to the source, and wherein the observer is fixed relative to the source.

Substituting equation (39) into (38),

$$S_{pp}(\omega) = \frac{1}{2\pi} \int_0^{2\pi} \left(\frac{\omega'}{\omega}\right)^2 S'_{pp}(\omega', \gamma)\, d\gamma. \tag{40}$$

The above result agrees with Schlinker and Amiet,[7] provided that ω is replaced by ω_o in the left hand side of equation (54) in their report, and *omega* and *omega*$_o$ are swapped in the left hand side of their equation (56). Note that the exponent of 2 in the Doppler term of equation (40) is not the only one found in the literature. Amiet[18] initially proposed a value of 1 for the exponent. Rozenberg et al[8] use an exponent of 1. Blandeau et al[11] use an exponent of -2.

IV. Kim-George's approach for rotating blades

Kim and George[10] have combined the exact solution for a rotating point source, from Ffowcs-Williams,[19] with Amiet's isolated airfoil theory,[3,12] to predict the sound pressure level radiating by turbulence past the trailing edge of a rotating blade.

A. Harmonic solution of the convected wave equation

The pressure field generated by an unsteady lift force per unit area $\mathbf{L}(\mathbf{x}, t)$ over an airfoil is given by:[20]

$$p(\mathbf{x_o}, t) = -\int_{-\infty}^{+\infty} \int_\Sigma \nabla G(\mathbf{x}, \tau | \mathbf{x}_o, t) \cdot \mathbf{L}(\mathbf{x}, \tau)\, d\Sigma\, d\tau, \tag{41}$$

where Σ is the blade planform and G a free field Green's function which satisfies

$$\left(\nabla_o^2 - \frac{1}{c_0^2}\frac{D_o^2}{Dt^2}\right) G(\mathbf{x},\tau|\mathbf{x}_o,t) = -\delta(t-\tau)\delta(\mathbf{x_o}-\mathbf{x}), \tag{42}$$

where $D_o/Dt = \partial/\partial t - U_z\partial/\partial z_o$.

If we define the Fourier transform pair $(f,\tilde{f})$ as

$$\tilde{f}(\omega) = \frac{1}{2\pi}\int_{-\infty}^{+\infty} f(t)e^{-i\omega t}\,dt, \tag{43}$$

$$f(t) = \int_{-\infty}^{+\infty} \tilde{f}(\omega)e^{i\omega t}\,d\omega, \tag{44}$$

then taking the inverse Fourier transform of equation (41) over time t yields

$$\tilde{p}(\mathbf{x_o},\omega) = -\int_{-\infty}^{+\infty}\int_{\Sigma} \nabla\tilde{G}(\mathbf{x},\tau|\mathbf{x}_o,\omega)\cdot\mathbf{L}(\mathbf{x},\tau)\,d\Sigma\,d\tau. \tag{45}$$

Taking the Fourier transform over time t of equation (42) gives

$$\left(\nabla_o^2 - \left(ik - M_z\frac{\partial}{\partial z_o}\right)^2\right)\tilde{G}(\mathbf{x},\tau,|\mathbf{x}_o,\omega) = -\frac{1}{2\pi}e^{-i\omega\tau}\delta(\mathbf{x_o}-\mathbf{x}), \tag{46}$$

where $k = \omega/c_0$. If we look for solutions of the above equation in the form

$$\tilde{G}(\mathbf{x},\tau|\mathbf{x}_o,\omega) = \frac{e^{-i\omega\tau}}{2\pi}\tilde{G}_\omega(\mathbf{x}|\mathbf{x}_o), \tag{47}$$

we find that $G_\omega(\mathbf{x}|\mathbf{x}_o)$ must be a solution of the following equation:

$$\left(\nabla_o^2 - \left(ik - M_z\frac{\partial}{\partial z_o}\right)^2\right)\tilde{G}_\omega(\mathbf{x}|\mathbf{x}_o) = -\delta(\mathbf{x_o}-\mathbf{x}), \tag{48}$$

Substituting (48) into (45) gives

$$p(\mathbf{x_o},\omega) = -\int_{\Sigma}\int_{-\infty}^{+\infty} \nabla\tilde{G}_\omega(\mathbf{x}|\mathbf{x}_o)\cdot\frac{1}{2\pi}\mathbf{L}(\mathbf{x},\tau)e^{-i\omega\tau}\,d\tau\,d\Sigma \tag{49}$$

B. Frequency Domain Green's function

A solution to equation (48) is given by[21]

$$\tilde{G}_\omega(\mathbf{x}|\mathbf{x}_o) = -\frac{i}{8\pi}\sum_{n=-\infty}^{+\infty} e^{-in(\gamma_o-\gamma)}\int_{-\infty}^{+\infty} J_n(\beta r)H_n^{(2)}(\beta r_o)e^{-ik_z(z_o-z)}\,dk_z, \tag{50}$$

where $\beta = \sqrt{(k+k_zM_z)^2 - k_z^2}$, J_n is the Bessel function of the first kind of order n, $H_n^{(2)}$ is the Hankel function of the second kind of order n and $r_o = \sqrt{x_o^2+y_o^2}$.

In the far field, we have

$$H_n^2(\beta r_o) \approx \sqrt{\frac{2}{\pi\beta r_o}}e^{-i\beta r_o + in\pi/2 + i\pi/4}, \tag{51}$$

so equation (50) can be written

$$\tilde{G}_\omega(\mathbf{x}|\mathbf{x}_o) = \sum_{n=-\infty}^{+\infty} e^{-in(\gamma_0-\gamma)}e^{-in\psi}I_{k_z}(r,z,r_o,z_o), \tag{52}$$

where γ is the azimuthal angle of the blade leading edge (assumed to be in the rotor plane), $\gamma - \psi$ the azimuthal angle of $\mathbf{x}$ (the source position along the blade is not at angle γ since the blade is not orthogonal to the rotor plane, as shown in figure 10), and

$$I_{k_z}(r, z, r_o, z_o) = -\frac{i}{8\pi} e^{i\pi/4} \int_{-\infty}^{+\infty} \sqrt{\frac{2}{\pi\beta r_o}} J_n(\beta r) \exp\{-i[\beta r_o + k_z(z_o - z) - n\pi/2]\}\, dk_z. \quad (53)$$

Defining the emission coordinates $r_o = R_e \sin\theta_e$ and $z_o = R_e(\cos\theta_e - M_z)$, and using the method of stationary phase, we find that the wavenumber of stationary phase k_{zs} is given by

$$k_{zs} = \frac{k\cos\theta_e}{1 - M_z\cos\theta_e}, \quad (54)$$

and

$$I_{k_z} \approx \frac{\exp[i(k_{zs}z + n\pi/2 - kR_e)]}{4\pi R_e(1 - M_z\cos\theta_e)} J_n\left(\frac{kr\sin\theta_e}{1 - M_z\cos\theta_e}\right) \quad (55)$$

Pressure field in frequency domain

Using cylindrical coordinates (r, γ, z),

$$\mathbf{L} = (\cos\alpha\, \mathbf{e_z} - \sin\alpha\, \mathbf{e}_\gamma)\, L, \quad (56)$$

$$\nabla\tilde{G}_\omega = \sum_{n=-\infty}^{+\infty} \left(\frac{\partial}{\partial r}\mathbf{e_r} + \frac{in}{r}\mathbf{e}_\gamma + ik_{zs}\mathbf{e_z}\right) e^{-in(\gamma_0-\gamma)} e^{-in\psi} I_{k_z}, \quad (57)$$

$$\nabla\tilde{G}_\omega \cdot \mathbf{L} = \sum_{n=-\infty}^{+\infty} i\left(k_{zs}\cos\alpha - \frac{n}{r}\right) e^{-in(\gamma_0-\gamma)} e^{-in\psi} I_{k_z}. \quad (58)$$

Substituting (58) into (49),

$$p(\mathbf{x_o}, \omega) = -\int_\Sigma \int_{-\infty}^{+\infty} \sum_{n=-\infty}^{+\infty} i\left(k_{zs}\cos\alpha - \frac{n}{r}\right) e^{-in\gamma_0} e^{-in\psi} I_{k_z} \frac{1}{2\pi} L(\mathbf{x}, \tau) e^{-i(\omega\tau - n\gamma)}\, d\tau\, d\Sigma \quad (59)$$

If Ω denotes the rotor rotational speed, then the blade is located at $\gamma = \Omega\tau$ and,

$$p(\mathbf{x_o}, \omega) = -\int_\Sigma \sum_{n=-\infty}^{+\infty} i\left(k_{zs}\cos\alpha - \frac{n}{r}\right) e^{-in\gamma_0} e^{-in\psi} I_{k_z} \tilde{L}(\mathbf{x}, \omega - n\Omega)\, d\Sigma, \quad (60)$$

where we have introduced the Fourier transform in time of the lift $\tilde{L}$.

We now introduce the blade source coordinates (r, X), which can be expressed in terms of z and ψ from figure 10:

$$r\psi = (c + X)\cos\alpha, \qquad z = (c + X)\sin\alpha, \quad (61)$$

where c is the blade chord.

Substituting equations (54), (55) and (61) into (62) yields

$$p(\mathbf{x_o}, \omega) = -\frac{i\exp(-ikR_e)}{4\pi R_e(1 - M_z\cos\theta_e)} \sum_{n=-\infty}^{+\infty} \int_r \int_c^0 S_n J_n\left(\frac{kr\sin\theta_e}{1 - M_z\cos\theta_e}\right) e^{-in(\gamma_0 - \pi/2)} e^{-i(k_c X + \phi_s)} \times \tilde{L}(r, X, \omega - n\Omega)\, dr\, dX, \quad (62)$$

where

$$S_n = \frac{k\cos\theta_e}{1 - M_z\cos\theta_e}\cos\alpha - \frac{n}{r}\sin\alpha, \quad (63)$$

$$k_c = \frac{k\cos\theta_e}{1 - M_z\cos\theta_e}\sin\alpha - \frac{n}{r}\cos\alpha, \quad (64)$$

$$\phi_s = k_c c. \quad (65)$$

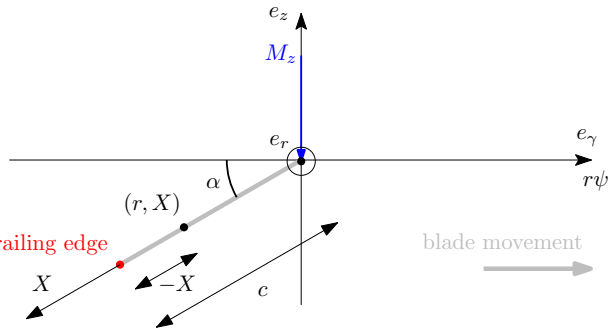

Figure 10: Blade source coordinates (r, X) as a function of z and ψ.

C. Acoustically weighted lift

The lift is equal to the pressure jump generated by a distribution of turbulent gusts $P(k_X, k_r)$, i.e.

$$L(X, r, t) = \int_{-\infty}^{+\infty} \int_{-\infty}^{+\infty} P(k_X, k_r) g_0(X, k_X, k_r) e^{ik_X U_c t - ik_r r} \, dk_X \, dk_r, \tag{66}$$

where g_0 is the blade response function defined as

$$g_0 = \left[(1+i)E^*[-X(k_X + M_X\mu + \xi)] + e^{\epsilon k_X X} - 1\right] e^{-ik_X X}, \tag{67}$$

where

$$\mu = \frac{M_X k_x}{\beta^2}, \qquad k_x = \frac{\omega}{U_r}, \qquad \xi = \frac{\sqrt{k^2 - \beta^2 k_r^2}}{\beta^2}, \qquad \beta^2 = 1 - M_X^2. \tag{68}$$

Taking the Fourier transform of (66) gives

$$\tilde{L}(X, r, \omega) = \int_{-\infty}^{+\infty} \int_{-\infty}^{+\infty} P(k_X, k_r) g_0(X, k_X, k_r) \delta(k_X U_c - \omega) e^{-ik_r r} \, dk_X \, dk_r \tag{69}$$

$$= \int_{-\infty}^{+\infty} \int_{-\infty}^{+\infty} P(k_X, k_r) g_0(X, k_X, k_r) \frac{1}{U_c} \delta(kx - \omega/U_c) e^{-ik_r r} \, dk_X \, dk_r \tag{70}$$

$$= \int_{-\infty}^{+\infty} \frac{1}{U_c} P(\omega/U_c, k_r) g_0(X, \omega/U_c, k_r) e^{-ik_r r} \, dk_r. \tag{71}$$

Substituting the lift equation (71) into (62) yields

$$p(\mathbf{x_o}, \omega) = -\frac{i \exp(-ikR_e)}{4\pi R_e (1 - M_z \cos\theta_e)} \sum_{n=-\infty}^{+\infty} \int_r \int_{-\infty}^{+\infty} S_n J_n \left(\frac{kr \sin\theta_e}{1 - M_z \cos\theta_e} \right)$$
$$e^{-in(\gamma_0 - \pi/2)} e^{-i\phi_s} P(K_X, k_r) \Psi_L(X, K_X, k_r, k_c) e^{-ik_r r} \, dk_r \, dr, \tag{72}$$

where

$$K_X = \omega - n\Omega \tag{73}$$

and Ψ is the acoustically weighted lift defined in equation (6)

D. Power spectral density

The pressure power spectral density is defined as

$$S_{pp}(\mathbf{x}_o, \omega) = \lim_{T \to +\infty} \frac{\pi}{T} E[p(\mathbf{x}_o, \omega) p^*(\mathbf{x}_o, \omega)], \tag{74}$$

where E denotes the expected value.

Substituting (74) in (72) gives

$$S_{pp}(\mathbf{x}_o,\omega) = \left(\frac{1}{4\pi R_e(1-M_z\cos\theta_e)}\right)^2 \sum_{m=-\infty}^{+\infty}\sum_{m'=-\infty}^{+\infty} e^{i(m'-m)\pi/2}\times$$
$$\int_{R_h}^{R_t}\int_{R_h}^{R_t}\int_{-\infty}^{+\infty}\int_{-\infty}^{+\infty} \frac{S_n S_n'}{U_c U_c'} e^{i(k_r r - k_r' r')}\Psi_L^*\Psi_L' J_m\left(\frac{kr\sin\theta_e}{1-M_z\cos\theta_e}\right) J_{m'}\left(\frac{kr'\sin\theta_e}{1-M_z\cos\theta_e}\right)$$
$$e^{i(\phi_s-\phi_s')} e^{ik_r(r-r')} \lim_{T\to+\infty}\frac{\pi}{T} E[p(\mathbf{x}_o,\omega)p^*(\mathbf{x}_o,\omega)]\, dk_r\, dk_r'\, dr'\, dr. \quad (75)$$

It can be shown that

$$\lim_{T\to+\infty}\frac{\pi}{T}E[p(\mathbf{x}_o,\omega)p^*(\mathbf{x}_o,\omega)] = U_c\delta(k_r'-k_r)\delta_{m,m'}\Phi_{qq}(K_X,k_r), \quad (76)$$

where Φ_{qq} is the turbulence energy spectrum. Substituting (76) in (75) leads to

$$S_{pp}(\mathbf{x}_o,\omega) = \left(\frac{1}{4\pi R_e(1-M_z\cos\theta_e)}\right)^2 \sum_{m=-\infty}^{+\infty}\int_{R_h}^{R_t} I_{m0}\, dr, \quad (77)$$

where

$$I_{m0} \equiv \int_{-\infty}^{+\infty} I_{m1}\Phi_{qq}(K_x,k_r)\, dk_r, \quad (78)$$

$$I_{m1} \equiv \int_{R_h}^{R_t} \frac{S_1}{U_c} S_1'\Psi_L^*\Psi_L' J_m(k_e r)\, J_m(k_e r')\, e^{i(\Phi_s-\Phi_s')} e^{ik_r(r-r')}\, dr', \quad (79)$$

and $k_e = k\sin\theta_e/(1-M_z\cos\theta_e)$. We assume that only the eddies that are within a small radial strip of width $\Delta r \ll r$ (slightly larger than the correlation length l_r) are correlated. In this narrow trip, the flow variables can be considered constant in the amplitude terms of equation (79)(S_1, S_1', U_c and U_c'): they are equal to their values at $r = r'$. For simplicity, given the complex nature of the phase in Ψ, we also assume $\Psi = \Psi'$, which gives

$$I_{m1} \approx \frac{S_1^2}{U_c}|\Psi_L(K_x,k_c,k_r)|^2 \int_{r-\Delta r/2}^{r+\Delta r/2} J_m(k_e r)\, J_m(k_e r')\, e^{i(\Phi_s-\Phi_s')} e^{ik_r(r-r')}\, dr' \quad (80)$$

$$I_{m1} \approx \frac{S_1^2}{U_c}|\Psi_L(K_x,k_c,k_r)|^2 J_m(k_e r)\, P_m, \quad (81)$$

where, letting $\eta = r' - r$ and using the first order approximation

$$\Phi_s' \approx \Phi_s + \frac{m\cos\alpha}{r^2}\eta, \quad (82)$$

$$P_m = \int_{-\Delta r/2}^{+\Delta r/2} J_m(k_e(\eta+r))\, e^{-i(k_r - mc\cos\alpha/r^2)\eta}\, d\eta. \quad (83)$$

The integral form of the second J_m term is given by[22]

$$J_m(k_e(\eta+r)) \equiv \frac{1}{2\pi}\int_{-\pi}^{\pi} e^{i(m\gamma - k_e(\eta+r)\sin\gamma)}\, d\gamma. \quad (84)$$

Substituting (84) into (83),

$$P_m = \frac{1}{2\pi}\int_{-\pi}^{\pi} e^{i(m\gamma - k_e r\sin\gamma)} \int_{-\Delta r/2}^{+\Delta r/2} e^{-i(k_r - mc\cos\alpha/r^2 + k_e\sin\gamma)\eta}\, d\eta\, d\gamma. \quad (85)$$

If Δr is large relative to the wavelengths of interest in this problem, i.e. if $k_r\Delta r \gg 1$, then the second integral in (85) simplifies to

$$\int_{-\infty}^{+\infty} e^{-i(k_r - mc\cos\alpha/r^2 + k_e\sin\gamma)\eta}\, d\eta = 2\pi\delta(k_r - k_{r0}), \quad (86)$$

where

$$k_{r0} = mc\cos\alpha/r^2 - k_e\sin\gamma. \tag{87}$$

Substituting (86) into (79), we get

$$I_{m1} = \frac{S_1^2}{U_c} J_m\left(k_e r\right) \int_{-\pi}^{\pi} |\Psi(K_x, k_c, k_r)|^2 e^{i(m\gamma - k_e r\sin\gamma)} \delta(k_r - k_{r0})\, d\gamma. \tag{88}$$

Substituting (88) into (89) gives

$$I_{m0} = \frac{S_1^2}{U_c} J_m\left(k_e r\right) I_{m2} \tag{89}$$

where

$$I_{m2} = \int_{-\pi}^{\pi} e^{i(m\gamma - k_e r\sin\gamma)} \int_{-\infty}^{+\infty} |\Psi(K_x, k_c, k_r)|^2 \Phi_{qq}(K_x, k_r)\delta(k_r - k_{r0})\, dk_r\, d\gamma, \tag{90}$$

$$I_{m2} = \int_{-\pi}^{\pi} e^{i(m\gamma - k_e r\sin\gamma)} |\Psi(K_x, k_c, k_{r0})|^2 \Phi_{qq}(K_x, k_{r0})\, d\gamma. \tag{91}$$

The integral I_{m2} is of the form

$$I_{m2} = \int_{-\pi}^{\pi} e^{ik_e r h(\gamma)} f(\gamma) d\gamma\, d\gamma, \tag{92}$$

where $h(\gamma) \equiv m/(k_e r)\gamma - \sin\gamma$ and where $f(\gamma)$ varies slowly with γ. The phase of the complex exponential in (92) varies quickly with γ for large values of $k_e r$, i.e. at high frequency (and for $\theta_e \neq 0$). Most of the contribution to the integral comes from the angle γ_s where the phase is stationary, i.e. where $h'(\gamma_s) = 0$. The angle γ_s exists if $|m| \leq k_e r$ and is given by

$$\gamma_s = \arccos\left(\frac{m}{k_e r}\right). \tag{93}$$

If $|m| \leq k_e r$ We therefore approximate I_{m2} by

$$I_{m2} \approx f(\gamma_s) \int_{-\pi}^{\pi} e^{ik_e r h(\gamma)} d\gamma\, d\gamma, \tag{94}$$

$$I_{m2} \approx |\Psi(K_x, k_c, k_{rs})|^2 \Phi_{qq}(K_x, k_{rs}) \int_{-\pi}^{\pi} e^{i(m\gamma - k_e r\sin\gamma}\, d\gamma, \tag{95}$$

$$I_{m2} \approx 2\pi |\Psi(K_x, k_c, k_{rs})|^2 \Phi_{qq}(K_x, k_{rs}) J_m(k_e r), \quad (|m| \leq k_e r), \tag{96}$$

where we have used the Bessel integral of equation (84), and where

$$k_{rs} = mc\cos\alpha/r^2 - k_e\sin\gamma_s. \tag{97}$$

For $|m| \geq k_e r$, equation (92) can be used for computing I_{m2}.

Substituting (96) into (89),

$$I_{m0} \approx \frac{S_1^2}{U_c} \begin{cases} 2\pi J_m\left(k_e r\right)^2 |\Psi(K_x, k_c, k_{rs})|^2 \Phi_{qq}(K_x, k_{rs}), & \text{if} \quad |m| \leq |k_e| r, \\ 0 & \text{if} \quad |m| \geq 1.1|k_e| r, \\ J_m\left(k_e r\right) \displaystyle\int_{-\pi}^{\pi} e^{i(m\gamma - k_e r\sin\gamma)} |\Psi(k_{r0})|^2 \Phi_{qq}(k_{r0})\, d\gamma, & \text{otherwise.} \end{cases} \tag{98}$$

Equation (98) allows to compute the PSD at the observer location when combined with equation (77).

The turbulence wavenumber spectrum Φ_{qq} is related to the power spectrum S_{qq} by

$$\Phi_{qq}(K_X, k_r) = \frac{U_c}{\pi} S_{qq}(\omega - m\Omega) l_r(\omega - m\Omega, k_r), \tag{99}$$

so that

$$I_{m0} \approx S_1^2 \begin{cases} 2J_m\left(k_e r\right)^2 |\Psi(K_x, k_c, k_{rs})|^2 S_{qq}(K_x U_c) l_r(k_{rs}), & \text{if} \quad |m| \le |k_e| r, \\ 0 & \text{if} \quad |m| \ge 1.1|k_e| r, \\ \dfrac{1}{\pi} J_m\left(k_e r\right) \displaystyle\int_{-\pi}^{\pi} e^{i(m\gamma - k_e r \sin\gamma)} |\Psi(k_{r0})|^2 S_{qq}(K_x U_c) l_r(k_{r0})\, d\gamma, & \text{otherwise.} \end{cases} \tag{100}$$

Substituting (100) into (77),

$$S_{pp}(\mathbf{x}_o, \omega) = \left(\frac{1}{4\pi R_e (1 - M_z \cos\theta_e)} \right)^2 \sum_{|m| \le 1.1|k_e r|} \int_{R_h}^{R_t} I_{m0}(r)\, dr, \tag{101}$$

For a small blade element of width Δr, the above equation reduces to

$$S_{pp}(\mathbf{x}_o, \omega) = \frac{\Delta r}{(4\pi R_e (1 - M_z \cos\theta_e))^2} \sum_{|m| \le 1.1|k_e r|} I_{m0}(r). \tag{102}$$

V. Results

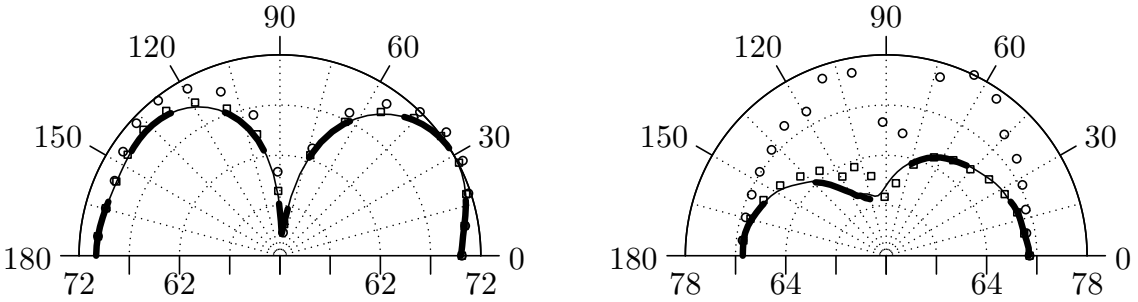

(a) Wind turbine (b) Open propeller at takeoff.

Figure 11: Sound pressure directivity using Amiet's approach and Kim-George's approach (dashed line), when the exponents of the Doppler shift in Amiet's approach (equation (40)) equals -2 ($\circ$ symbols), 1 ($\square$ symbols), and 2 (solid line). The frequency is set to $kc = 5$.

Figure 11 compares the sound pressure directivity obtained using Kim-George's approach and Amiet's approach, when the exponents of the Doppler shift (see equation (40)) takes the values 1, 2 and -2. These values are the ones that appear in the literature. A low Mach number case (wind turbine) is shown in figure 11(a), and high Mach number case is shown in fugure 11(b). The best agreement between Kim-Georges approach and Amiet's approach is obtained for an exponent of 2 (+ symbols), which validates equation (40).

Figures 14–13 show the sound pressure directivity, for the rotors defined in table 2, which are simple models for an open propeller at take-off (figure 14) and cruise (figure 15), a cooling fan (figure 12) and a wind turbine (figure 13). In each figure, the results are obtained using the Kim-George approach (dashed line) and the Amiet apprach (solid line).

The two approaches give identical results for a wind turbine and a cooling fan. They agree to within 1 dB for the open propeller during take-off. Some discrepancies of up to 3 dB can be observed for the open propeller at cruise (figure 15), over the whole frequency range. The discrepancies for $0° \le \theta \le 90°$ can be explained by the fact that, for these angles, the Doppler shift almost goes to 0 for some values of γ (because the chordwise Mach number M_{ch} is so close to 1 as shown in table 2), in which case the source frequency ω' tends to 0. The very low frequencies cannot be estimated accurately using the high frequency blade response function, so we expect Amiet's approach to become less accurate in this case. It is not clear what the origin of the dip is for $\theta \ge 90°$, but it is aligned with the blade (i.e. it is at $\theta = \pi/2 + \alpha$).

	Cooling fan	Wind turbine	Open propeller
radius	0.40 m	29 m	1.80 m
chord	0.13 m	2 m	0.31 m
M_t	0.0525	0.165	0.748
α	34 deg	10 deg	13 deg (take-off), 38 deg (cruise)
M_z	0.0354	0.029	0.584 (take-off), 0.228 (cruise)
M_{ch}	0.0633	0.167	0.949 (take-off), 0.782 (cruise)

Table 2: Typical parameters for the rotors used in three different applications: open-propeller, cooling fan and wind turbine. These parameters are the ones proposed by Blandeau and Joseph.[11] Note that M_z and M_{ch} are a function of α and M_t; they are given for completeness.

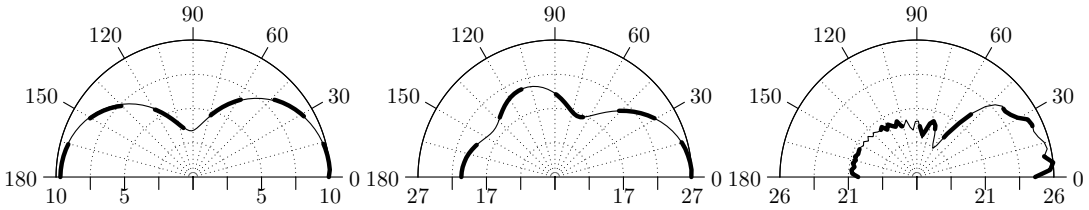

(a) $kc = 0.5$ (b) $kc = 5$ (c) $kc = 50$

Figure 12: Sound pressure level for a cooling fan. Solid line is Amiet's approach, dashed line Kim-George's approach. Wind speed is from right to left.

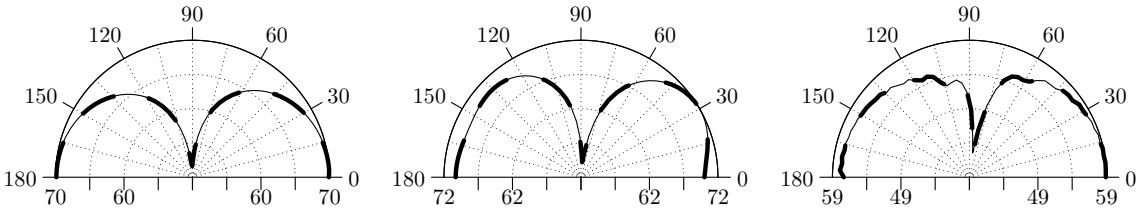

(a) $kc = 0.5$ (b) $kc = 5$ (c) $kc = 50$

Figure 13: Sound pressure level for a Wind turbine. Solid line is Amiet's approach, dashed line Kim-George's approach. Wind speed is from right to left.

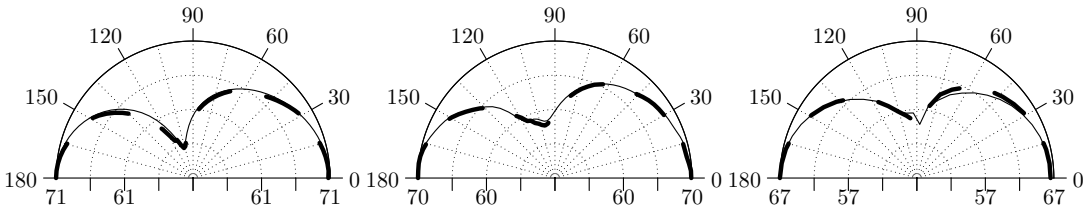

(a) $kc = 0.5$ (b) $kc = 5$ (c) $kc = 50$

Figure 14: Sound pressure level for an open propeller take-off. Solid line is Amiet's approach, dashed line Kim-George's approach. Wind speed is from right to left.

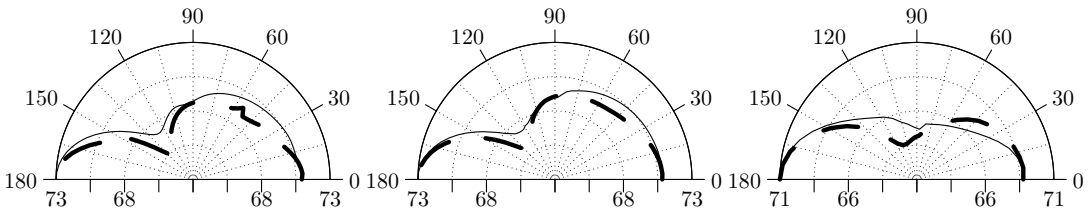

(a) $kc = 0.5$ (b) $kc = 5$ (c) $kc = 50$

Figure 15: Sound pressure level for an open propeller cruise. Solid line is Amiet's approach, dashed line Kim-George's approach. Wind speed is from right to left.

Conclusion

Amiet's theory[7] for predicting trailing noise from rotating blade has been validated by comparing it to a non-compact version of Kim-George's approach.[10] Amiet's theory is valid at high frequency $kc > 1$, and for low enough chordwise Mach numbers ($M_{ch} \leq 0.85$). Beyond this range, the two approaches differ by up to 3 dB.

The correct exponent for the Doppler term $(\omega'/\omega)^a$ in Amiet's theory is $a = 2$. Using $a = 1$, as in Amiet[6] and Rozenberg et al[8] gives results exact to within 1 dB. However, $a = -2$ overestimates the result by up to 10 dB.

The range of validity of Amiet's theory is currently limited to high frequencies because it uses a high frequency blade response function. It is likely to be equally valid at lower frequencies, provided that a low frequency blade response function is used.[4]

Acknowledgements

Samuel Sinayoko and Anurag Agarwal wish to acknowledge the support of Mitsubishi Heavy Industries. Mike Kingan wishes to acknowledge the continuing financial support provided by Rolls-Royce plc. through the University Technology Centre in Gas Turbine Noise at the Institute of Sound and Vibration Research. The authors wish to thank Vincent Blandeau, Thomas Nodé-Langlois, Stephane Moreau, Michel Roger and Ann Dowling for their thoughtful comments.

References

[1]Amiet, R. K., "Acoustic radiation from an airfoil in a turbulent stream," *Journal of Sound and Vibration*, Vol. 41, No. 4, 1975, pp. 407–420.

[2]Amiet, R. K., "High frequency thin-airfoil theory for subsonic flow," *AIAA Journal*, Vol. 14, 1976, pp. 1076–1082.

[3]Amiet, R. K., "Noise due to turbulent flow past a trailing edge," *Journal of Sound and Vibration*, Vol. 47, No. 3, 1976, pp. 387–393.

[4]Roger, M. and Moreau, S., "Back-scattering correction and further extensions of Amiet's trailing-edge noise model. Part 1: theory," *Journal of Sound and Vibration*, Vol. 286, No. 3, 2005, pp. 477–506.

[5]Moreau, S. and Roger, M., "Back-scattering correction and further extensions of Amiet's trailing-edge noise model. Part II: Application," *Journal of Sound and Vibration*, Vol. 323, No. 1-2, 2009, pp. 397–425.

[6]Amiet, R. K., "Noise produced by turbulent flow into a propeller or helicopter rotor," *AIAA paper*, Vol. AIAA-76-56, 1976.

[7]Schlinker, R. H. and Amiet, R. K., "Helicopter rotor trailing edge noise," *AIAA, Astrodynamics Specialist Conference*, 1981.

[8]Rozenberg, Y., Roger, M., and Moreau, S., "Rotating Blade Trailing-Edge Noise: Experimental Validation of Analytical Model," *AIAA Journal*, Vol. 48, No. 5, 2010, pp. 951–962.

[9]Blandeau, V., *Aerodynamic Broadband Noise from Contra-Rotating Open Rotors*, Ph.D. thesis, University of Southampton, 2011.

[10]Kim, Y. N. and George, A. R., "Trailing-Edge Noise from Hovering Rotors," *AIAA Journal*, Vol. 20, No. 9, 1982, pp. 1167–1174.

[11]Blandeau, V. and Joseph, P., "Validity of Amiets Model for Propeller Trailing-Edge Noise," *AIAA Journal*, Vol. 49, No. 5, 2011, pp. 1057–1066.

[12]Amiet, R. K., "Effect of the incident surface pressure field on noise due to turbulent flow past a trailing edge," *Journal of Sound and Vibration*, Vol. 57, 1978, pp. 305–306.

[13]Brooks, T. F. and Hodgson, T. H., "Trailing edge noise prediction from measured surface pressures," *Journal of Sound and Vibration*, Vol. 78, 1981, pp. 69–117.

[14]Schlinker, R. H. and Amiet, R. K., "Helicopter rotor trailing edge noise," Tech. Rep. 1, NASA Contractor Report 3470, 1981.

[15]Ffowcs Williams, J. E. and Hawkings, D. L., "Sound generation by turbulence and surfaces in arbitrary motion," *Philosophical Transactions for the Royal Society of London. Series A, Mathematical and Physical Sciences*, Vol. 264, No. 1151, 1969, pp. 321–342.

[16]Howe, M. S., "Edge-source acoustic green's function for an airfoil of arbitrary chord, with application to trailing-edge noise," *The Quarterly Journal of Mechanics and Applied Mathematics*, Vol. 54, No. 1, 2001, pp. 139–155.

[17]Amiet, R. K., "Frame of Reference Considerations for the Forward Flight Noise Problem," Tech. rep., UARL Report N212775-1, 1974.

[18]Amiet, R. K., "Noise Produced by Turbulent Flow into a Propeller or Helicopter Rotor," *AIAA Journal*, Vol. 15, No. 3, 1977, pp. 307–308.

[19]Ffowcs-Williams, J. E., "The Noise from Turbulence Convected at High Speed," *Philosophical Transactions for the Royal Society of London. Series A, Mathematical and Physical Sciences*, Vol. 255, No. 1061, 1963, pp. 469–503.

[20]Goldstein, M. E., *Aeroacoustics*, McGraw-Hill International Book Co., 1976.

[21]Kingan, M. J., Powles, C., and Self, R. H., "Effect of Centerbody Scattering on Advanced Open-Rotor Noise," *AIAA Journal*, Vol. 48, No. 5, 2010, pp. 975–980.

[22]Abramowitz, M. and Stegun, I. A., editors, *(9.1) Bessel functions of integer order, in Handbook of Mathematical Functions with Formulas,Graphs, and Mathematical Tables, 9th printing*, Dover Publications, 1972.